Science Bulletin 64 (2019) 315–320

Contents lists available at ScienceDirect

Science Bulletin

journal homepage: www.elsevier.com/locate/scib

Article

The contribution of photoinduced charge-transfer enhancement to the SERS of uranyl(VI) in a uranyl-Ag_2O complex

Shaofei Wang [a], Shanli Yang [a], Haoxi Wu [a], Jiaolai Jiang [a], Lang Shao [a], Yiming Ren [a], Yingru Li [a], Chuanhui Liang [a], Mingfu Chu [a], Xiaolin Wang [b,*]

[a] Institute of Materials, China Academy of Engineering Physics, Jiangyou 621907, China
[b] China Academy of Engineering Physics, Mianyang 621900, China

ARTICLE INFO

Article history:
Received 29 November 2018
Received in revised form 9 January 2019
Accepted 28 January 2019
Available online 2 February 2019

Keywords:
Photoinduced charge-transfer
Uranyl
SERS
Ag_2O aggregates
Trace analysis

ABSTRACT

Charge-transfer (CT) is an important enhancement mechanism in the field of surface-enhanced Raman scattering (SERS) that typically increases the Raman intensity of molecules by as much as 10–100 times. Herein, a low-cost Ag_2O aggregates substrate was prepared via a facile chemical precipitation method, and the calculated CT-based enhancement factor of the uranyl ions adsorbed on it reached as high as 10^5, a metal-comparable value. The efficient photoinduced CT process from the valence band of Ag_2O to the LUMO of uranyl ions under appropriate excitation sources resulted in the repulsion of the axial oxygen atoms of the O=U=O bond, which enhanced its polarizability, creating a more intense Raman mode. To the best of our knowledge, this study firstly reports such a strong photoinduced CT enhancement of uranyl ions, with concentrations of 10^{-8} mol L^{-1} or lower being detected using this Ag_2O substrate. Most importantly, this research has shown that the photoinduced CT enhancement also contributes to the SERS of uranyl ions on pure Ag substrates which have often been ascribed to the electromagnetic enhancement in previous studies. In addition, Ag_2O can be used to selectively detect uranyl ions without interference from many other molecules or ions because of the energy matching rule of the photoinduced CT process, which was readily available for uranyl detection in the environmental aqueous solution.

1. Introduction

Uranyl (UO_2^{2+}) is one of the most common radioactive pollutants in the environment, and the concerns about its environmental effects and threats to human health have steadily increased over time [1–4]. Hence, there is an urgent need to precisely and rapidly monitor the content of uranyl ions in environmental aqueous settings, which has resulted in the rapid development of many different uranyl detection methods, such as colorimetric methods [5–7], fluorescence methods [8,9], mass spectrometry [10–12], and electrochemistry [13,14]. Due to its fast response, high sensitivity, and its successful application in the rapid trace analysis of biological molecules [15–17], organic pollutants [18–22], and heavy metal ions [23,24], SERS is expected to become an alternative technique for the detection of uranyl. Currently, many studies have reported the SERS of uranyl ions, and the employed SERS substrates are mainly based on Ag nanostructures, such as Ag nanorods arrays [25,26], Ag nanoparticles [27–29], Ag-doped sol-gel film [30], etc. These Ag nanostructures have been shown to produce significant Raman enhancements from the uranyl ions located close to their surfaces, which contributes to the trace analysis of uranyl ions. To achieve a maximum improvement in the Raman intensity of uranyl ions, it is necessary to understand the SERS mechanism of uranyl ions on the Ag nanostructures. Although there is some debate, most researchers currently agree that the Raman enhancement is mainly attributed to two things: electromagnetic (EM) enhancement derived from laser-inducing local surface plasma resonance of noble metal nanostructures [31], and chemical enhancement caused by a charge-transfer complex (between the substrate and target molecule) resonating with the excitation source [32]. Of the two, the former is generally regarded as the dominant factor, and the resulting enhancement factor is usually about 10^6 or higher [33]. Consequently, previous studies about the SERS of uranyl ions have mainly focused on the preparation of the Ag substrate with high-density "hotspots" to improve the EM effect. "Hotspots" are the sites that possess large electromagnetic field and usually exist in closely-packed nanostructures that are separated by nanoscale dielectric gaps. However, few studies

* Corresponding author.
E-mail address: xlwang@caep.cn (X. Wang).

https://doi.org/10.1016/j.scib.2019.01.025
2095-9273/

systematically investigated the charge-transfer (CT) enhancement mechanism for the SERS of uranyl ions on Ag substrates. Hence, it is very important to investigate the contribution of the CT mechanism to the Raman enhancement.

As the CT enhancement and EM enhancement jointly contribute to the SERS of uranyl ions on Ag substrates, it is difficult to distinguish between the individual contribution of each one. Hence, a substitute that only produces a CT enhancement is needed. Herein, Ag_2O was used as the substitute for Ag substrates for the following reasons: (1) the CT enhancement is independent of the geometric configuration of the Ag substrate but is related to the chemical reaction that it undergoes with uranyl; (2) the equatorial plane of uranyl coordinates with Ag_2O via an oxo-bridge geometry, namely U-O-Ag, which was also observed for the uranyl ions adsorbed on the Ag substrates [27,28]; (3) since it is a p-type semiconductor, the surface plasma resonance frequency of Ag_2O lies in the infrared region, far from 532/638/785 nm excitation lines used in this research, which should effectively exclude the EM enhancement from the Ag_2O substrate. Therefore, to deeply understand the CT enhancement on the Ag substrate, the photoinduced CT process in a uranyl-Ag_2O complex was thoroughly discussed using experimental and theoretical results to offer explanations.

In this study, a substrate based on Ag_2O aggregates was synthesized via a facile chemical precipitation method and characterized using X-ray diffraction (XRD) and scanning electron microscopy (SEM) to determine its atomic structure and surface morphology. The photoinduced CT mechanism of uranyl ions on the Ag_2O, as well as its contribution to Raman enhancement was studied in detail. In addition, the SERS spectra of uranyl at different concentrations were also investigated, and it was found that as low as 10^{-8} mol L^{-1} could be easily detected. These results indicate that the SERS technique based on Ag_2O aggregates presented favorable application prospects for rapidly monitoring trace uranyl ions in the environment.

2. Experimental

2.1. Reagents

Silver nitrate, titanium dioxide, zinc oxide, rhodamine 6G, and crystal violet were purchased from Aladdin Chemical Company. Hydrochloric acid, sodium hydrate, H_2O_2 (30%), and other reagents were obtained from Chengdu Kelong Chemical Company of China. All reagents were analytically pure and used as received without any further purification. Deionized water (18.2 MΩ) was used for sample dilutions throughout the experiment.

2.2. Apparatus

Raman scattering spectra were obtained using a Horiba XploRA Raman spectrometer with 532, 638, and 785 nm lasers attached to an upright microscope. A 50 × objective was used to focus the laser beam (~4 μm in diameter) on the Ag_2O substrate to collect Raman signals. Before data acquisition, the instrument was calibrated with standardized silicon according to a routine procedure, and the laser powers incident on the sample surface were measured using the instrument's self-contained power meter (Table 1).

Table 1
The laser powers to the sample surface.

	532 nm	638 nm	785 nm
10% laser Power	0.76 mW	0.78 mW	1.72 mW
100% laser Power	5.97 mW	6.37 mW	14.17 mW

XRD was conducted on a PANalytical Empyrean advance X-ray diffractometer equipped with a PIXcel^{3D} detector (Cu Kα radiation at 40 mA and 40 kV, λ = 1.5406 Å), with a 2θ scanning range of 30°–90°. SEM characterization was conducted using a SIRION 200 scanning electron microscope.

2.3. Synthesis of Ag_2O and uranyl chloride

Silver nitrate (0.05 g) was dissolved in 5 mL of deionized water, and then 5 mL of sodium hydrate solution (0.1 mol L^{-1}) was slowly added with rough agitation. A brown AgOH colloid was rapidly generated, and aggregates were quickly formed due to the accumulation of colloidal particles. The aggregates were then washed with enough deionized water to remove the residual sodium, silver, and nitrate ions. Subsequently, the AgOH was mixed with 2 mL deionized water and exposed to air for 24 h to form brownish black Ag_2O aggregates. Finally, the as-prepared Ag_2O was preserved at room temperature and away from light.

Hydrochloric acid solution (5 mL, 5 mol L^{-1}) was heated to 70 °C, and then 0.238 g of high-purity uranium-238 was added, followed by the dropwise addition of 2 mL of H_2O_2 (30%). Uranium was completely dissolved after 5 min, which was continuously heated until its volume was reduced to 3 mL. Subsequently, the residual solution was diluted to 100 mL using deionized water. Finally, 10^{-2} mol L^{-1} uranyl chloride stock solution was obtained, and dilute solutions (10^{-8}–10^{-3} mol L^{-1}) were prepared by diluting the stock solution.

2.4. Raman measurements

The as-prepared Ag_2O aggregates were well dispersed in 2 mL of deionized water through ultrasonic shaking, and then 2 μL of the dispersion was dropped onto the silicon wafer and dried at room temperature. Subsequently, 2 μL of the uranyl chloride solution was dropped onto the Ag_2O, and the Raman signals were collected after the evaporation of water at room temperature.

To detect low concentrations of uranyl chloride, 5 μL of the Ag_2O aggregates suspension was added into 4 mL of the uranyl chloride solution, and then the mixture was shaken for 1 h. The Ag_2O was then taken out and dried at room temperature and was analyzed by Raman spectroscopy. The Raman measurements method for rhodamine 6G and crystal violet on the Ag_2O aggregates was identical to uranyl chloride.

3. Results and discussion

XRD and SEM were used to characterize the atomic composition, structure, and morphology of the Ag_2O aggregates. As shown in Fig. 1a, the XRD pattern of the as-prepared Ag_2O aggregates was consistent with the standard XRD pattern of Ag_2O (JCPDS No. 41-1104). The peaks at 32°, 38°, 55°, and 66° were attributed to the (1 1 1), (2 0 0), (2 1 1), and (2 2 2) planes of the cubic Ag_2O crystal phase, respectively. The characteristic diffraction peaks of Ag (2 0 0) and Ag (3 1 1) were not observed, which indicates that there was no metallic silver doped in the as-prepared Ag_2O aggregates. SEM image (Fig. 1b) indicated that the Ag_2O had a loose and porous structure with large sizes that ranged from several hundred nanometers to micron dimensions. The purpose of using large Ag_2O aggregates as the substrate was to prevent the occurrence of EM enhancement as much as possible, which can be easily produced when small Ag_2O nanoparticles are irradiated by laser.

It has been reported that the SERS activity of Ag_2O is essentially contributed by the Ag particles generated from the photochemical reduction during laser excitation [34]. In other words, EM enhancement should be responsible for the SERS effect. In this study, the

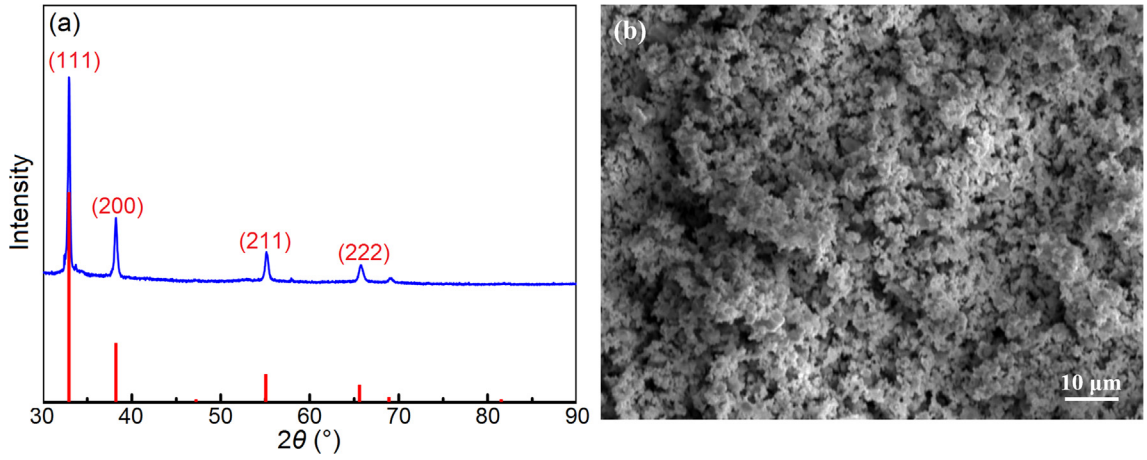

Fig. 1. (Color online) (a) XRD pattern of the as-prepared Ag_2O aggregates (blue, upper) and the standard XRD pattern of Ag_2O (JCPDS No. 41-1104) (red, lower). (b) SEM image of the as-prepared Ag_2O aggregates.

Raman spectra of uranyl chloride, rhodamine 6G, and crystal violet adsorbed on the Ag_2O aggregates were compared with each other to confirm the specific SERS mechanism. As shown in Fig. 2, no characteristic Raman signals were observed for rhodamine 6G or crystal violet as the laser irradiation time increased, while a strong band located at 715 cm^{-1} appeared for uranyl chloride. It is well-known that rhodamine 6G and crystal violet are typically used as Raman probing molecules to evaluate the EM enhancement of Ag substrates, hence neither of their Raman signals could exclude the EM enhancement derived from the laser-irradiated Ag_2O aggregates. Thus, the Raman enhancement of uranyl ions adsorbed on the Ag_2O aggregates probably resulted from the CT effect, which led to the serious weakening of the O═U═O bond and thus its large red-shift from 870 cm^{-1} (the normal Raman band of O═U═O(ν_1) for free uranyl chloride) to 715 cm^{-1}. In addition, the Raman intensity of uranyl showed a gradual increase as the laser irradiation time increased, reaching a maximum at 9 min, which indicated that the CT reaction in the uranyl-Ag_2O complex rapidly reached equilibrium. Herein, the accuracy of previous reports concerning the generation of Ag particles through the photochemical reduction process is not questioned. However, this report notes that the EM enhancement of the laser-irradiated Ag_2O aggregates could be ignored due to the large-scale structures of Ag_2O and the low laser power used in this study.

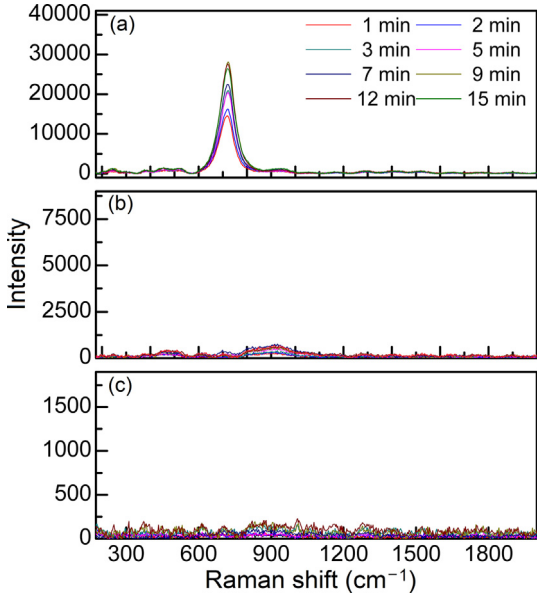

Fig. 2. (Color online) Laser irradiation time dependence of Raman spectra of Ag_2O aggregates after immersion in 4 mL of 10^{-6} mol L^{-1} uranyl chloride (a), 10^{-5} mol L^{-1} rhodamine 6G (b), and 10^{-5} mol L^{-1} crystal violet (c). Laser excitation: 532 nm; 100% laser power; accumulation time: 10 s.

The occurrence of a photoinduced CT process mainly depends on the exciting laser energy being no lower than the energy difference between Ag_2O and the uranyl ion. Herein, the valance band (VB) and conduction band (CB) of Ag_2O are −5.89 and −4.69 eV [35], respectively, and the HOMO and LUMO of the uranyl ion are −10.39 and −4.06 eV, respectively [36]. In Scheme 1, an energy level diagram is used to illustrate the CT mechanism in detail. The possible CT process that occurred between Ag_2O and the uranyl ion includes four modes: (1) electrons from the VB of Ag_2O are directly excited to the LUMO of the uranyl ion by the exciting laser with an energy no less than 1.83 eV; (2) electrons from the VB of Ag_2O are excited to the CB by an exciting laser with an energy no less than 1.2 eV and are then injected into the LUMO of the uranyl ion; (3) electrons from the HOMO of the uranyl ion are directly excited to the CB of Ag_2O by the exciting laser with an energy no less than 5.70 eV; (4) electrons from the HOMO of the uranyl ion are excited to the LUMO by the exciting laser with an energy no less than 6.33 eV and are then injected into the CB of Ag_2O. It's obvious that mode 3 and 4 cannot occur since the exciting lasers of 532, 638, and 785 nm (ca. 2.33, 1.94, and 1.58 eV, respectively)

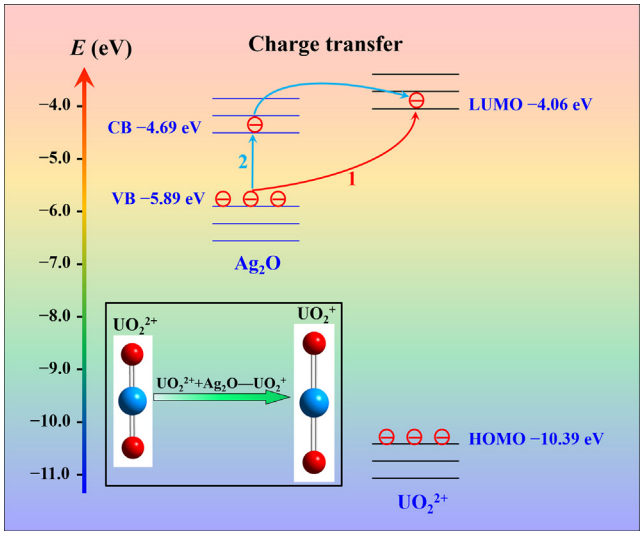

Scheme 1. (Color online) Schematic diagram of the photoinduced CT process between Ag_2O and uranyl ion.

do not have sufficient energy to excite the electron transitions from the HOMO of the uranyl ion to its own LUMO or to the CB of Ag_2O. However, 532 nm and 638 nm meet the requirements for modes 1 and 2, while 785 nm is only feasible for mode 2. Hence, the photoinduced charge-transfer from Ag_2O to the uranyl ion occurred, leading to the reduction of uranyl(VI) to uranyl(V).

As shown in Fig. 3, large Raman enhancements of uranyl ions adsorbed on Ag_2O occurred at excitation wavelengths of 532 and 638 nm, while a very weak Raman signal was observed for 785 nm. Hence, this result confirmed the major contribution of mode 1 to the Raman enhancements. As shown in Scheme 1, electron is excited from the VB of Ag_2O to its CB and then to the LUMO of the uranyl ion in mode 2, while electron is directly excited from the VB of Ag_2O to the LUMO of the uranyl ion in mode 1. Hence, mode 1 has a higher charge-transfer efficiency than mode 2, which results in the large Raman enhancements of the uranyl ion at the excitation wavelengths of 532 and 638 nm and the weak Raman signal when using the 785 nm laser. In addition, the SERS signal at the excitation wavelength of 532 nm is stronger than that at 638 nm because of the more efficient CT process at the higher laser energy.

The specific contribution of the photoinduced CT effect to the Raman enhancement of uranyl ions was evaluated using the apparent enhancement factor (EF). As shown in Fig. 4, the EF value can be calculated from the difference of the Raman intensity of the O=U=O(ν_1) band between the SERS of uranyl chloride adsorbed on the Ag_2O aggregates and the normal Raman of uranyl chloride. Herein, the peak area of O=U=O(ν_1) was used as the criterion for its Raman intensity. The original Raman spectra were processed using a baseline calibration, and then the treated spectra were fitted to obtain peak areas using the self-contained calculation program of the Raman instrument. Finally, the EF value was obtained by using the following formula:

$$EF = I_S[C_R]P_R t_R / I_R[C_S]P_S t_S,$$

where I, C, P, and t represent the peak area of O=U=O(ν_1), the concentration of uranyl chloride, laser power, and accumulation time, respectively. Their subscripts, S and R, represent SERS and normal Raman respectively. Surprisingly, the calculated value could reach up to 10^5, which is a metal-comparable EF value. It is generally accepted that the conventional CT process results in a 10 to 100 times signal enhancement [37], which is much lower than the value obtained in the current study. As mentioned above, the O=U=O(ν_1) band was shifted from 870 to 715 cm^{-1} when the uranyl ion was adsorbed on the Ag_2O aggregates. This large red-shift indicated the considerable weakening of the O=U=O bond derived from the efficient photoinduced CT effect from the VB of Ag_2O to the LUMO of the uranyl ion. Consequently, the polarizability of O=U=O showed a significant increase, as did its Raman intensity.

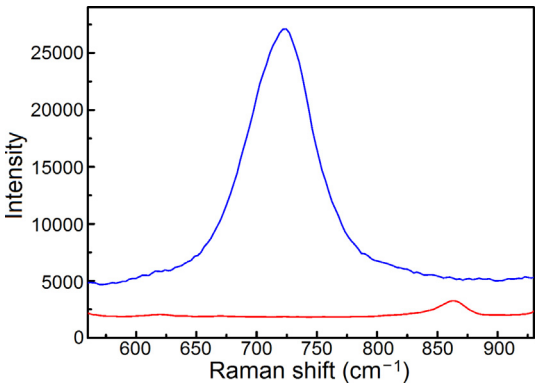

Fig. 4. (Color online) Normal Raman spectrum of 0.05 mol L^{-1} uranyl chloride (2 μL, red line) and SERS of 10^{-5} mol L^{-1} uranyl chloride (2 μL, blue line) adsorbed on the Ag_2O aggregates. Laser excitation: 532 nm; power: 100%; accumulation time: 10 s.

The ground state CT effect that arises from the chemical bonding between the uranyl ion and metallic oxides is well-known to also promote the Raman intensity of O=U=O(ν_1). Hence, to further confirm that the photoinduced CT effect, rather than the ground state CT effect, was responsible for the Raman enhancement, two metallic oxides with strong adsorption affinities for uranyl ions were chosen as the substrates to investigate the Raman enhancement of uranyl ions. The two oxides were TiO_2 (VB: −7.41 eV; CB: −4.21 eV) and ZnO (VB: −7.39 eV; CB: −4.19 eV), which are both commonly used as SERS substrates [38–40]. As shown in Fig. 5, when compared to the Raman signals of the uranyl ions adsorbed on Ag_2O, only very weak Raman peaks between 800 and 855 cm^{-1} were observed for even higher concentrations of uranyl ions adsorbed on TiO_2 and ZnO. The strong Raman bands centered at 394, 515, and 637 cm^{-1} belong to the characteristic vibrations of TiO_2. This phenomenon is likely due to the energy of the 532 nm laser (2.33 eV) being unable to excite the charge-transfer from the VB of TiO_2 and ZnO to their own CB or to the LUMO of the uranyl ion since the energy gaps are greater than 2.33 eV. Consequently, the requirement for the generation of the photoinduced CT process was not met, and much poorer Raman enhancements of the uranyl ion on TiO_2 and ZnO were completely a result of the ground state CT effect. Hence, this result further con-

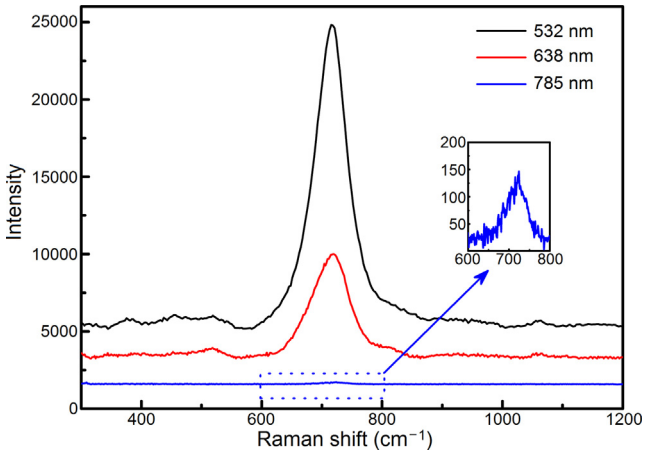

Fig. 3. (Color online) Raman spectra of 10^{-4} mol L^{-1} uranyl chloride (2 μL) adsorbed on the Ag_2O aggregates at the excitation wavelengths of 532, 638, and 785 nm, respectively. Laser power: 10% for 532 and 638 nm, 100% for 785 nm; accumulation time: 10 s.

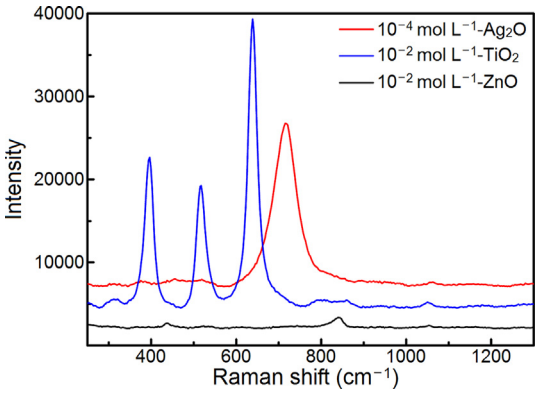

Fig. 5. (Color online) Raman spectra of uranyl chloride (2 μL) adsorbed on TiO_2 and ZnO in comparison with that adsorbed on the Ag_2O aggregates. Laser excitation: 532 nm; 10% laser power; accumulation time: 10 s.

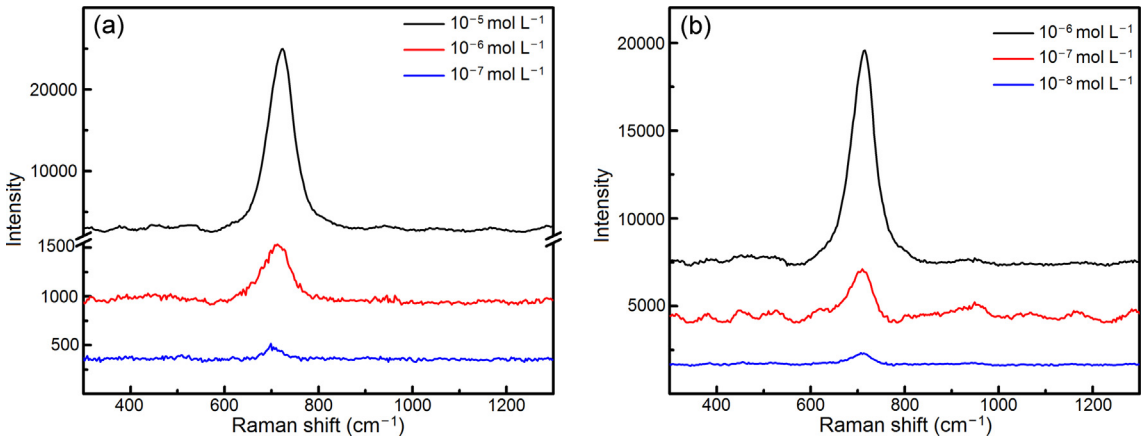

Fig. 6. (Color online) (a) Raman spectra of uranyl chloride (2 μL; 10^{-7}, 10^{-6}, and 10^{-5} mol L^{-1}) adsorbed on the Ag_2O aggregates. (b) Raman spectra of Ag_2O aggregates after immersion in 4 mL of uranyl chloride (10^{-8}, 10^{-7}, and 10^{-6} mol L^{-1}). Laser excitation: 532 nm; 100% laser power; accumulation time: 10 s.

firmed that the photoinduced CT effect was responsible for the Raman enhancement of the uranyl ions adsorbed on the Ag_2O aggregates. Additionally, Raman enhancement from the ground state CT effect occurred independently from the excitation lasers, hence why weaker Raman signals were produced from the uranyl ions adsorbed on the Ag_2O aggregates at the 785 nm laser compared to 532 and 638 nm. This also suggested the rather small contribution of the ground state CT effect to the Raman enhancement.

Previous studies have also observed an intense Raman enhancement of uranyl ions adsorbed on Ag substrates with a O═U═O(ν_1) band located at ~710 cm^{-1}, and ascribed this enhancement to an efficient EM effect [25,27,30]. However, this study firstly demonstrates that the photoinduced CT effect can also tremendously contribute to the Raman enhancement. It is known that the oxidation of Ag atoms can significantly decrease the surface plasma resonance intensity of Ag substrates, which reduces the EM enhancement effect. Nevertheless, the generated Ag_2O also provides a huge CT enhancement, as well as an excellent adsorption affinity for the uranyl ions. Consequently, when the oxidation of Ag atoms reaches a certain extent, the combination of CT and EM mechanisms potentially produces a more intense Raman enhancement on the Ag substrates.

The high EF value made the trace analysis of uranyl ions feasible. As shown in Fig. 6, the Raman spectra of different concentrations of uranyl chloride on the Ag_2O aggregates were obtained in this study, which indicated that a uranyl chloride concentration of 10^{-8} mol·L^{-1} could be detected. It is likely that even lower concentrations of uranyl chloride can be detected through its sufficient enrichment on Ag_2O. Compared to previous studies that have reported the SERS measurements of uranyl on Ag substrates, this method demonstrated several advantages: (1) the extremely simple and facile preparation process of Ag_2O aggregates; (2) the detectability of the uranyl ions on the Ag_2O aggregates substrate was equal to or better than that on the Ag substrates, while hardly any background or interfere signals were observed, which significantly improved the detection accuracy; (3) the long-term stability of the Ag_2O aggregates was much better than the reported Ag substrates; (4) most importantly, the energy matching rule of a photoinduced CT process made the selective detection of uranyl ions possible, which was extremely favorable for the uranyl detection in the complex environmental aqueous solution.

4. Conclusion

The photoinduced CT process from the VB of Ag_2O to the LUMO of the uranyl ions occurred when appropriate excitation sources were used. This resulted in the repulsion of the axial oxygen atom of the O═U═O bond, which increased its polarizability, allowing it to produce a much more intense Raman mode. The calculated photoinduced CT-based EF value of uranyl ions adsorbed on the Ag_2O aggregates reached as high as ~10^5, which is 3–4 orders of magnitude greater than the established value obtained from conventional CT enhancement. Previous studies have reported that the intensive Raman enhancement of uranyl ions adsorbed on Ag substrates was caused by the EM effect. However, this study firstly demonstrates that the CT effect can also provide a tremendous contribution, and hence to further increases the knowledge of the SERS mechanism of uranyl ions. Due to the strong CT enhancement, the aqueous solutions containing uranyl chloride with concentrations of 10^{-8} mol L^{-1} or lower could be detected using Ag_2O aggregates. Most importantly, the energy matching rule of the CT process made it possible for selective detecting uranyl ions in complex aqueous solutions, which suggests excellent application prospects for the rapid monitoring of uranyl ions in the environment.

Conflict of interest

The authors declare that they have no conflict of interest.

Acknowledgments

This work was supported by the Development Foundation of Radiochemistry (XK 909) of China Academy of Engineering Physics (CAEP), the National Natural Science Foundation of China (21501157, 21504085), the Science Challenge Project (TZ2016000403), Sichuan Science and Technology Foundation for Young Scientists (2017JQ0050), and Foundation for Special Talents in CAEP (TP201502-3).

Author contributions

Shaofei Wang designed and carried out the experiment. Shanli Yang and Haoxi Wu conducted the data collation and analysis. Jiaolai Jiang participated in the preparation of silver oxide substrate. Lang Shao performed the XRD characterization of silver oxide and evaluated its composition. Yiming Ren and Yingru Li conducted the SEM characterization and explained the structure and morphology of silver oxide. Chuanhui Liang performed the XPS characterization and investigated the main components of silver oxide. Mingfu Chu reviewed and revised the paper. Xiaolin Wang provided the guidance for the whole research process and wrote the paper with Shaofei Wang.

Appendix A. Supplementary data

Supplementary data to this article can be found online at https://doi.org/10.1016/j.scib.2019.01.025.

References

[1] Prat O, Vercouter T, Ansoborlo E, et al. Uranium speciation in drinking water from drilled wells in southern Finland and its potential links to health effects. Environ Sci Technol 2009;43:3941–6.
[2] Clark DL, Hobart DE, Neu MP. Actinide carbonate complexes and their importance in actinide environmental chemistry. Chem Rev 1995;95:25–48.
[3] Lan JH, Chai ZF, Shi WQ. A combined DFT and molecular dynamics study of U (VI)/calcite interaction in aqueous solution. Sci Bull 2017;62:1064–73.
[4] Yang DX, Wang XX, Song G, et al. One-pot synthesis of arginine modified hydroxyapatite carbon microsphere composites for efficient removal of U(VI) from aqueous solutions. Sci Bull 2017;62:1609–18.
[5] Hu L, Yan XW, Li Q, et al. Br-PADAP embedded in cellulose acetate electrospun nanofibers: colorimetric sensor strips for visual uranyl recognition. J Hazard Mater 2017;329:205–10.
[6] Zhu JH, Zhao X, Yang JD, et al. Selective colorimetric and fluorescent quenching determination of uranyl ion via its complexation with curcumin. Spectrochim Acta A 2016;159:146–50.
[7] Zhang DY, Chen Z, Omar H, et al. Colorimetric peroxidase mimetic assay for uranyl detection in sea water. ACS Appl Mater Interfaces 2015;7:4589–94.
[8] Maji S, Viswanathan KS. Enhancement of uranyl fluorescence using trimesic acid: ligand sensitization and co-fluorescence. J Lumin 2011;131:1848–52.
[9] Chen WM, Meng XL, Zhuang GL, et al. A superior fluorescent sensor for Al^{3+} and UO_2^{2+} based on a Co(II) metal-organic framework with exposed pyrimidyl Lewis base sites. J Mater Chem A 2017;5:13079–85.
[10] Luo MB, Hu B, Zhang X, et al. Extractive electrospray ionization mass spectrometry for sensitive detection of uranyl species in natural water samples. Anal Chem 2010;82:282–9.
[11] Crawford CL, Fugate GA, Cable-Dunlap PR, et al. The novel analysis of uranyl compounds by electrospray-ion mobility-mass spectrometry. Int J Mass Spectrom 2013;333:21–6.
[12] Li Y, Yang ML, Sun R, et al. Detection of uranium in industrial and mines samples by microwave plasma torch mass spectrometry. J Mass Spectrom 2016;51:159–64.
[13] Ziolkowski R, Gorski L, Malinowska E. Carboxylated graphene as a sensing material for electrochemical uranyl ion detection. Sensor Actuat B Chem 2017;238:540–7.
[14] Tang Q, Yuan YL, Xiao XL, et al. DNAzyme based electrochemical sensors for trace uranium. Microchim Acta 2013;180:1059–64.
[15] Zhao YQ, Huang JA, Zhang ZY, et al. Quantitative analysis of multiplex-components and double stranded DNA by wide-range surface-enhanced Raman spectroscopy based on ordered Ag/Si nanowire arrays. J Mater Chem A 2014;2:10218–24.
[16] Kho KW, Dinish US, Kumar A, et al. Frequency shifts in SERS for biosensing. ACS Nano 2012;6:4892–902.
[17] Kang T, Yoo SM, Yoon I, et al. Patterned multiplex pathogen DNA detection by Au particle-on-wire SERS sensor. Nano Lett 2010;10:1189–93.
[18] Zhao HY, Jin J, Tian WJ, et al. Three-dimensional superhydrophobic surface-enhanced Raman spectroscopy substrate for sensitive detection of pollutants in real environments. J Mater Chem A 2015;3:4330–7.
[19] Bharadwaj S, Pandey A, Yagci B, et al. Graphene nano-mesh-Ag-ZnO hybrid paper for sensitive SERS sensing and self-cleaning of organic pollutants. Chem Eng J 2018;336:445–55.
[20] Li XH, Chen GY, Yang LB, et al. Multifunctional Au-coated TiO_2 nanotube arrays as recyclable SERS substrates for multifold organic pollutants detection. Adv Funct Mater 2010;20:2815–24.
[21] Zhang HH, Zhou F, Liu M, et al. Spherical nanoparticle arrays with tunable nanogaps and their hydrophobicity enhanced rapid SERS detection by localized concentration of droplet evaporation. Adv Mater Interfaces 2015;2:1500031.
[22] Zhang HH, Liu M, Zhou F, et al. Physical deposition improved SERS stability of morphology controlled priodic micro/nanostructured arrays based on colloidal templates. Small 2015;11:844–53.
[23] Zeng Y, Ren J, Shen AG, et al. Field and pretreatment-free detection of heavy-metal ions in organic polluted water through an alkyne-coded SERS test kit. ACS Appl Mater Interfaces 2016;8:27772–8.
[24] Kim K, Lee JW, Shin KS. Cyanide SERS as a platform for detection of volatile organic compounds and hazardous transition metal ions. Analyst 2013;138:2988–94.
[25] Leverette CL, Villa-Aleman E, Jokela S, et al. Trace detection and differentiation of uranyl(VI) ion cast films utilizing aligned Ag nanorod SERS substrates. Vib Spectrosc 2009;50:143–51.
[26] Wang SF, Zou SM, Yang SL, et al. HfO_2-wrapped slanted Ag nanorods array as a reusable and sensitive SERS substrate for trace analysis of uranyl compounds. Sensor Actuat B Chem 2018;265:539–46.
[27] Bhandari D, Wells SM, Retterer ST, et al. Characterization and detection of uranyl ion sorption on silver surfaces using surface enhanced Raman spectroscopy. Anal Chem 2009;81:8061–7.
[28] Wang SF, Jiang JL, Wu HX, et al. Self-assembly of silver nanoparticles as high active surface-enhanced Raman scattering substrate for rapid and trace analysis of uranyl(VI) ions. Spectrochim Acta A 2017;180:23–8.
[29] Dutta S, Ray C, Sarkar S, et al. Silver nanoparticle decorated reduced graphene oxide (rGO) nanosheet: a platform for SERS based low-level detection of uranyl ion. ACS Appl Mater Interfaces 2013;5:8724–32.
[30] Bao LL, Mahurin SM, Haire RG, et al. Silver-doped sol-gel film as a surface-enhanced Raman scattering substrate for detection of uranyl and neptunyl ions. Anal Chem 2003;75:6614–20.
[31] Otto A, Futamata M. Electronic mechanisms of SERS. Top Appl Phys 2006;103:147–82.
[32] Musumeci A, Gosztola D, Schiller T, et al. SERS of semiconducting nanoparticles (TiO_2 hybrid composites). J Am Chem Soc 2009;131:6040–1.
[33] Jeanmaire DL, Surface Vanduyne RP. Raman spectroelectrochemistry. 1. heterocyclic, aromatic, and aliphatic-amines adsorbed on anodized silver electrode. J Electroanal Chem 1977;84:1–20.
[34] Xiao Y, Li YS, Swihart GH. A close look at silver oxide colloid for surface-enhanced Raman scattering. Talanta 2002;58:755–60.
[35] Butler MA, Ginley DS. Prediction of flatband potentials at semiconductor-electrolyte interfaces from atomic electronegativities. J Electrochem Soc 1978;125:228–32.
[36] Wang XX, Fan QH, Yu SJ, et al. High sorption of U(VI) on graphene oxides studied by batch experimental and theoretical calculations. Chem Eng J 2016;287:448–55.
[37] Ling X, Xie LM, Fang Y, et al. Can graphene be used as a substrate for Raman enhancement? Nano Lett 2010;10:553–61.
[38] Rumyantseva A, Kostcheev S, Adam PM, et al. Nonresonant surface-enhanced Raman scattering of ZnO quantum dots with Au and Ag nanoparticles. ACS Nano 2013;7:3420–6.
[39] Yang LB, Qin XY, Jiang X, et al. SERS investigation of ciprofloxacin drug molecules on TiO_2 nanoparticles. Phys Chem Chem Phys 2015;17:17809–15.
[40] Wang XT, Shi WX, Jin Z, et al. Remarkable SERS activity observed from amorphous ZnO nanocages. Angew Chem Int Ed 2017;56:9851–5.

Shaofei Wang is currently carrying out the graduate work for his doctor's degree under the guidance of Professor Xiaolin Wang at China Academy of Engineering Physics. His major research interest focuses on the surface enhanced Raman scattering of uranyl compounds.

Xiaolin Wang is a Research Professor and Deputy Director of the Science and Technology Committee at China Academy of Engineering Physics (CAEP). He received a B.Sc. in Radiochemistry from Sichuan University (China) in 1985, a M.Sc. in Nuclear Chemistry from CAEP in 1988, and a Ph.D. in Nuclear Material from CAEP in 1997. His main research interests include nuclear chemistry, radioanalytical chemistry and nuclear materials.